UNIVERSITY OF CALIFORNIA SAN DIEGO

Adhesion of Metal Thin Film on Polymeric Micro-Needle Substrate for Electrochemical Sensing Applications

A thesis submitted in partial satisfaction of the

requirements for the degree Master of Science

in

Materials Science and Engineering

by

Allison Furmidge

Committee in charge:

Professor Joseph Wang, Chair

Professor Prabankar Bandaru

Professor Patrick Mercier

2021

The thesis of Allison Furmidge is approved, and it is acceptable in quality and form for publication on microfilm and electronically.

University of California San Diego

2021

DEDICATION

In recognition of reading this manual before beginning to format the master's thesis; for following the instructions written herein; for consulting with the Graduate Division Academic Affairs Advisers; and for not relying on other completed manuscripts, this manual is dedicated to all graduate students about to complete the master's thesis.

In recognition that this is my one chance to use whichever justification, spacing, writing style, text size, and/or text font that I want to while still keeping my headings and margins consistent.

EPIGRAPH

If you look for truth, you may find comfort in the end: if you look for comfort you will not get either comfort or truth -- only soft soap and wishful thinking to begin with and, in the end, despair.

C.S. Lewis

TABLE OF CONTENTS

LIST OF ABBREVIATIONS

ISF: Interstitial fluid

Pt: Platinum

Cr: Chromium

Ti: Titanium

PMMA: Polymethyl-methacrylate

PLA: Polylactide

CNC: Computerized Numerical Control

DNA: Deoxyribonucleic Acid

LIST OF FIGURES

LIST OF TABLES

ACKNOWLEDGEMENTS

I would like to acknowledge Dr. Joseph Wang for all of his support in being my advisor and P.I. over the last year and a half, especially throughout the time of being completely remote due to covid. I would also like to acknowledge Farshad Tehrani for not only guiding me through the microneedle projects but being pivotal in my transition to take charge in the fabrication efforts. I would also like to thank Nickey Huang and Bale Nie for their assistance in etching, electrode isolation and adding covers to the sensors. I would also like to acknowledge various lab members such as Hazhir Teymourian, Jonathan Kavner, Reza Aghavali, Andres Duvvuri, and Tatiana Podhajny for their advice, mentorship, and assistance in teaching me the CNC.

ABSTRACT OF THE THESIS

Adhesion of Metal Thin Film on Polymeric Micro-Needle Substrate for Electrochemical Sensing Applications

by

Allison Furmidge

Master of Science in Materials Science and Engineering

University of California San Diego, 2021

Professor Joseph Wang, Chair

Over the last two decades, the field of electrochemical sensors has seen rapid growth in its functionality, accuracy, and miniaturization. There is a growing use of different nanostructures for enhancing the electrochemical detection, the integration of electrochemical sensing platforms with wearable bioelectronic technology, and multiplexed sensing with various biomarkers found in saliva, sweat, tears and ISF. The nanostructure of focus is microneedles, spread out on three different surfaces of electrodes: the working electrode, the reference electrode, and the counter electrode. These surfaces will consist of three main components that will be tested for electrochemical activity: the substrate roughness, the metallic coating, and the electrode layer interface thickness. This paper will be focusing on the interactions between the metallic coating adhesion between the layers to best optimize the performance and life of the sensor. Specifically, this paper will investigate different sputtered layer thicknesses of the electrode metals and its adhesion onto its PMMA or PLA substrate. This will be accomplished in three phases: cyclic voltammetry, physical adhesion promoters via the use of a 3D print and CNC

machine, and sputtering methods and protocols to help determine coating breakdown and rate of immobilization.

INTRODUCTION

Over the last two decades, the field of electrochemical sensors has seen rapid growth in its functionality, accuracy, and miniaturization around the world. Electrochemical sensors are a large subclass of chemical sensors that measure an analyte of interest with a recognition electrode to a signal transducer, creating reproducible results. This type of sensor has been shown to have a wide range of applications in various fields of medicine, agriculture, and industry. Smaller and more versatile electrochemical sensors have been developed that can noninvasively measure a wide range of specific biomarkers with remarkable results. These -micro and -nano level sensors can continuously screen for various analytes for the diagnosis of diseases, analysis of pesticides, monitoring of inflammatory pathways and much more. To develop these sensors with the best accuracy and efficacy, an essential important requirement to refine includes the metallic electrode layer and its corresponding substrate. By scaling down these sensors and modifying the electrode surface, interfering species can be controlled and avoided in the sensor, producing a lower sensitivity and more affinity for the analyte of interest.

There is a growing use of different nanostructures for enhancing the electrochemical detection, the integration of electrochemical sensing platforms with wearable bioelectronic technology, and multiplexed sensing with various biomarkers found in saliva, sweat, tears and ISF. The nanostructure of focus is microneedles, spread out on three different surfaces of electrodes: the working electrode, the reference electrode, and the counter electrode. These surfaces will consist of three main components: the substrate, the metallic coating, and the immobilization interface. In this thesis, we will begin with a review on these different interface layers commonly used on popular electrochemical sensors with an emphasis on human on-body

electrochemical sensing platforms, their methods of sensing, then investigate the use of current thin films and its application.

The best method of producing this electrode for sensing with varying sizes and shapes is to use both a substrate and a metallic thin film surface, with an adhesion layer in between to bond the two together. This provides a lightweight, robust, easily manufactured electrode compared to solely a metal or thin film surface. This also allows for more capability for surface modifications to provide better adhesion of the thin film to the substrate, as well as better analyte immobilization. Minimally invasive sensors will need to be highly biocompatible for a longer lasting electrode, and a thin film substrate surface will allow for flexibility in adjustments to the surface for specific analyte measurements.

The method of thin film adhesion to the substrate has an important effect on the life and reliability of an electrochemical sensor. There are multiple types of adhesion methods that we will explore in this paper, however the areas of interest for this experiment include different adhesion metals, thin film electrode layer thickness and physical modifications to the adhesion layer substrate. The biggest categories of adhesion include physical and chemical modifications, adding an adhesion layer to the substrate before depositing with the necessary electrode metals onto the surface. The sputter method with certain target materials such as chromium, titanium, and nickel prove itself to be very effective with argon gas. This works by using a plasma-based deposition process where high energy particles bombard the substrate and deposit a layer of desired metal. While this is commonly used in the semiconductor industry, this has been shown to be useful for depositing thin film electrodes for electrochemical sensors and biosensors due to its lack of impurities reaching the thin film. Typically, argon gas is used in the sputtering environment to reduce the amount of process gasses mixing with the target material on the

substrate. Once the substrate is placed in the sputtering vacuum and the normal atmospheric gas is replaced with a high-pressure argon gas, then the target material is ready for deposition. To get to the deposition, a negative charge is applied to the target material and a plasma around the target begins to glow. The argon and the target material begin a free electron exchange, ionizing argon and deionizing the target material. As these particles continue to collide with one another, target material atoms begin to bounce off the target material as the ionized argon continues to excite the target atoms, "sputtering" off the material. This will then create a very smooth, nano-thin sized film on the substrate[1].

The development for these multilayer sensors contains three main layers, with the substrate being the foundation and the majority of the sensor by volume. The PMMA substrate will be modified with the CNC machine, then will undergo a sputtering process in which the adhesion layer is placed first, then various layers of different metals used for the electrode itself. If the CNC machining is not used, then 3D printing will be used as an alternative to cut back on fabrication time and the manual labor required to make these. In this experiment, we will only use platinum as the electrode layer. Other metals such as gold, silver and aluminum have also been used for on-body sensing. Lastly, the immobilization layer is added on top of the electrode once the electrodes are separated mechanically either by the manufacturer or machining. Enzyme immobilization is extremely important for the accuracy and success of the biosensor. Careful engineering of the enzyme microenvironment (on the surface) can be used to greatly enhance the sensor performance. Compared to free enzymes in solution, immobilized enzymes are more robust and resistant to environmental changes. There are multiple ways to immobilize the analytes of interest, such as the common method of polymer entrapment, adsorption to the surface, as well as different types of covalent or biospecific binding to the surface. The scope of

this paper does not reach the electrochemical properties of the immobilization layer in relation to the adhesion layer, however this could be developed in further studies on this topic. The main focus of this paper will focus heavily on the adhesion layer and its succeeding electrode layer.

Thermoplastics have been widely used as substrates for their ease of manufacturing and accessibility. Synthetic polymers such as PMMA, PLA, and PDMS are common polymers. PMMA, or polymethyl-methacrylate, is the thermoplastic of interest due to its toughness, durability, and weight. These properties make PMMA very desirable for CNC applications, or a computer numerical control machine. When a piece of material is processed with a CNC, the CNC machine follows a coded programmed instruction without a manual operator directly controlling the machining operation, producing incredibly precise parts. In the application of a PMMA substrate, the CNC can help develop physically modified electrode surfaces with user-specific designs down to the micro-scale. This can include a rough surface, microneedle arrays, and physical electrode separation. PLA is similarly a good candidate for a substrate due to its ease of manufacturing when making intricate designs, such as all common 3D printing machines that use stereolithography printing. Stereolithography printing can create resolutions down to as low as 25 microns and generally creates a very streamline process with very little manual labor. For this experiment, Rigid 10K resin is used for this experiment, a photoinitiator mixed with urethane dimethacrylate, methacrylate monomers and a filler. This photoinitiator is essential for the stereolithography process, as the photoinitiator initiates cross-linking between the compounds in the resin, curing the resin to be a strong, tough solid[2]. While this resin is one of the strongest materials for 3D printing, no affordable 3D printer can reach the levels of resolution that only a CNC machine can achieve. While the Formlabs printers can reach layer heights as small as 20 microns, the CNC can reach as low as 1 micron resolution. While this may have no

effect on most electrochemical sensors and electrodes, this level of detail can largely determine the effectiveness and ability for the sensor to be able to penetrate through human skin. The place of interest is at the tip of the microneedles, where the sharpness of the microneedle tip is affected by the micron resolution.

Specifically for PMMA, this thermoplastic is attractive for many applications in nanotechnology and large-scale industry design. PMMA is synthesized through multiple polymerization methods to create a high resistance to sunlight and heat exposure. Due to its transparent nature and affordability, it can easily be found in modern structural designs, such as sheets, films, tubular and spherical composites. When handled properly, it does not release any toxic vapors and is safe to the touch. The biocompatibility and transparency of PMMA has opened opportunities for its use in injections, DNA microarrays, drug delivery and even cosmetics. PMMA has been increasingly utilized in the field of sensing as well, both being used on-body and as a liquid sensor using PMMA microspheres. Chemical vapor deposition has promising effects for thin film deposition onto PMMA and other polymers. However, PMMA on its own will not be sufficient as a substrate with common adhesion layers such as chromium or titanium, as the surface is extremely hydrophobic and will not be attracted to a hydrophilic metal. This means that it is necessary to add a coupling agent to enhance the adhesion layer and increase the longevity of the sensor as a whole. Without sufficient adhesion to the substrate, slight scratches and minimal use of the sensor will drastically inhibit electrochemical measurements or cause the sensor to fail completely. This paper will investigate various methods of surface modification and simulate the reliability of the adhesion layer for on-body applications. As PMMA works as both a rigid body and an adjustable surface, there are many different applications that involve skin penetration where these properties would be useful.

This experiment will focus on the method currently being developed for microneedle glucose sensor, a nearly $7 billion dollar industry worldwide and a significant portion of developing electrochemical on-body sensors. This method introduces the PMMA substrate modified with micro-CNC machining to develop a microneedle array around 150 microns in diameter connected to the counter, working and reference electrode. This unique sensor does not draw blood as many glucose measurements require; rather it measures multiple analytes from the interstitial fluid found in the skin cells just below the epidermis. This high-precision detail could only be performed with a micro-CNC, as other methods such as a 3D printer do not have the same level of precision and affordability as the CNC. These requirements become increasingly more demanding as more needles are added to the array, or if the diameter decreases. As more needles are added to expand the array, the needles can create a "bed-of-nails" effect. As the diameter decreases, the need for a more precise resolution determines its ability to penetrate the skin. With varying viscoelastic properties of the dermis and epidermis, a sharp tip will allow for ease of patient use without causing much pain.

Chromium has been characterized as one of the most valuable metals for thin layer adhesion on both polymeric and metallic surfaces in the semiconductor and biomedical industries. Its binding energy with oxygen allows the atoms to depassivate through many material surfaces, generating an interwoven locking mechanism with the chromium atoms and the substrate. The oxygen atoms act as the connecting bridge between the two materials, allowing even a large atom such as chromium to diffuse within many substrate materials. However, it is critical that there are no byproducts contaminating the surface or gas within the chamber as chromium is being deposited. As chromium locks with oxygen atoms, water vapor and hydrocarbons can form at high pressures and condense onto the substrate surface. When

using the sputtering machine, the argon gas is injected into the vacuum to avoid these byproducts and maintain as clean of a surface as possible.

Titanium is another strong candidate for an adhesion promoter. As another transition metal with only two more valence electrons, titanium acts very similar to silane coupling agents. Silane coupling agents use a Si-O branch to bridge the gap between silicon and another material. When looking at J.F. Hyde's diagram of the periodic table by valence electron notes as shown in Figure 1, a very similar comparison in spacing between the two. Dr. Edwin P. Plueddemann wrote about titanium-derived coupling agents, stating that titanium has a unique ability to generate an organic monomolecular layer on the substrate surface by interactions with free protons[3]. This slightly unstable layer on the surface, along with titanium valence structure, increases the substrate surface energy to create a strong bond. When these titanium-treated surfaces are incorporated with polymers, it can not only promote adhesion, but improve strength and mechanical properties, as well as preventing embrittlement. Titanium as an adhesion promoter has been tested to result in polymers with a higher tensile strength and elongation, producing a tougher polymer than those without an adhesion promoter or with a silane coupling agent. This may deem itself very useful when micron-sized detail is vital to the life and sustainability of the sensor on the body, as handling of the sensor can cause damage to the microneedles.

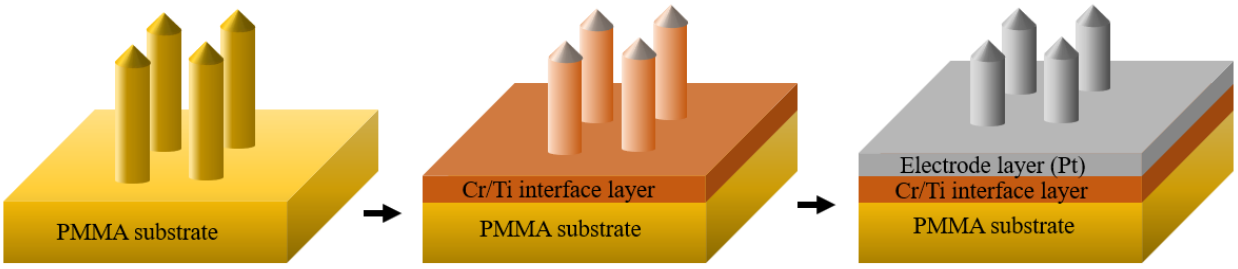

Figure 1. Layers of Electrode

The layering and thickness on the nano-scale can play a large role in the lifespan of the sensor. If the thickness of the electrode layers are too thin, then the electrode can be heavily altered by handling and mechanical manipulation of the sensor, causing unintended electrical discontinuity on the electrode surface. If the layers are too thick, then manufacturing prices can exponentially increase when using precious metals. Having too thick of any specific layer can also cause problems when the electrode surface is handled incorrectly, exposing unnecessary and potentially harmful metals to the human skin. Additionally, with this problem there is a possibility of causing an electrical short or discontinuity on any electrode. The thickness of the electrode layer in this experiment was determined by the previous experimentation performed by Joseph Wang et. al.[4] Certain ranges of layer thicknesses were calculated based on the previous ranges tested and tried. The low and the high end of each thickness used in this experiment approximates to about one standard deviation of the common range used in previous experiments.

Glucose oxidase does not directly transfer electrons to conventional electrodes because their redox center is surrounded by a thick protein layer, creating more space at the exchange site. The electron donor-acceptor pair will have too large of a spatial separation, and so it creates an intrinsic barrier to direct electron transfer. Improvements can be achieved by replacing the

oxygen with a non-physiological (synthetic) electron acceptor, which is able to shuttle electrons from the redox center of the enzyme to the surface of the working electrode. As a result of using artificial (diffusional) electron-carrying mediators, measurements become insensitive to oxygen fluctuations and can be carried out at lower potentials that do not provoke interfering reactions from coexisting electroactive species. The most common form of mediators is used with glucose oxidase, as shown in the bottom left. And as you can see on the right with the microneedles, that process is put into use with the TTF, which is an organic electron donor, that catalyzes the process from making gluconate from glucose[5].

One very important consideration in these electrochemical processes is to understand the capacitances and other impedances that arise when taking measurements on an imperfect surface. MAny scientists have been able to condense down these impedances into Randles circuit, a series combination circuit that consists of the ionic resistance from the surface and a parallel component with the double layer capacitance in parallel with the charge transfer resistance and the working electrode impedance, or the specific electrochemical element of diffusion called the Warburg element. The Warburg element is an impedance component that models the diffusion process at a constant phase of 45 degrees, or when the Bode plot curve has a slope of -½. This specific slope defines a linear relationship between the log of the impedance with the log of the frequency. We can assume that the electrode being tested in the experiment is large compared to the binding sites for the enzymes of interest, the equation assumes semi-infinite linear diffusion and we can assume that a Warburg constant exists. The circuit is defined in Figure 2 and is commonly used to help define the results of the impedance of electrochemical surfaces. By using electrochemical impedance spectroscopy, or EIS, we can break down the results of the Nyquist

and Bode plots obtained from EIS to describe the process and properties of an electrochemical interface[6].

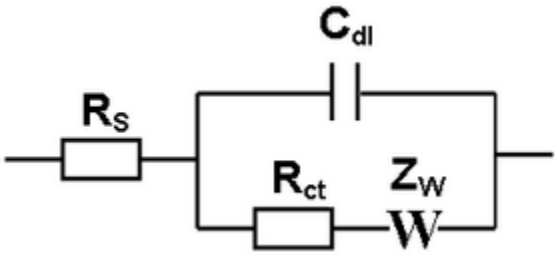

Figure 2. Randle's Circuit

Cyclic voltammetry is another test that will be run in conjunction with EIS. Cyclic voltammetry is a voltage-cycle test to measure the fluctuation of current as the voltage is increased and immediately reversed. This is ideal in many electrochemical applications as a linear potential sweep can catalyze charge transfer between the enzyme of interest and the electrode surface. Particularly in glucose sensing applications, this deems itself useful when glucose sensing relies heavily on the rate of charge transfer for more immediate response times. There are usually two peaks in a cyclic voltammetry graph, one on the positive voltage side and one on the negative[7].

CHAPTER 1. EXPERIMENT

The process began with creating and iterating a design with an 11-microneedle array structure, with seven microneedles on the reference electrode, three on the working electrode and one on the counter electrode. The design was completed on Fusion 360 with the dimensions developed in consideration of other working parts of a typical electrochemical glucose sensor, such as the PCBA, Qi coil, and battery. The height of the microneedles was determined based on the depth of the epidermis and the ability for the needles to maintain rigidity when under the force of penetration. The height of the microneedles was 1.3 microns, with ⅓ of the height being 100 microns larger in diameter than the rest of the needle to prevent breaking and maintain structural integrity. Once the CAD (computer-aided design) was complete, the computer-aided manufacturing was developed, or CAM. This CAM was developed in a series of steps that incorporated tool bit changes in the CNC, where the different tool bits will cut out parts of a 3 mm stock acrylic, placing a large emphasis on perfecting the microneedles. This began with cutting the majority of the acrylic around the microneedles, beginning with larger tool bits to decrease manufacturing time, then decreasing the tool bit size as the cuts reached closer to the microneedles themselves. Angled chamfer mills were used to make a high-precision cut around the microneedle tips. The last portion of the CNC cutting includes creating tabs around the sensor to prevent the microneedle sensor from completely separating from the acrylic stock, allowing for easier handling for the rest of the fabrication process. Up to 10 microneedle sensors can be developed by the CNC at once. In total, the CNC machining takes about 2 hours and 50 minutes to complete 10 microneedle sensors. During the sputtering process, the tabs are broken to remove the sensor from the acrylic stock. Due to much of the debris from the CNC cutting, the entire acrylic stock with the 10 sensors are washed with DI water and dried. After inspecting the

acrylic stock to ensure it is dry, the stock is placed on a metal sheet in the oven at 140 degrees Celsius for 8 hours in preparation for the sputtering process.

This process is very similar to the 3D printing method, where Fusion 360 is used to create the design. After the design is fully developed with CAD, an stl file is sent over to the Formlabs 3D printing software, Preform. A 3D print file is then sent to the Formlabs printer, and the entire process to print up to 12 microneedle sensors at once is around 8 hours. The 3D printing itself does not require manual assistance until it needs to be removed from the printer. Once removed, the 3D print is washed in 90% IPA for 30 minutes, dried for a few seconds, then rinsed again for another 30 minutes in a new 90% IPA wash. Then, it is placed in a UV curing chamber for 10 minutes. After this point, the 3D print is completely cured and free of any liquid resin covering the print. The supports holding the 3D print were removed with tweezers to isolate the microneedle sensor. The comparison of the 3D print and the CNC machine are shown in these SEM images below. Due to the 25 micron resolution of the 3D print compared to the 0.1 micron resolution of the CNC, the tips are much sharper and can allow for much smoother penetration on the CNC part than the 3D print.

For both the 3D printed and CNC machined sensors, both are placed into a sputtering chamber to add the thin film adhesion layer and the thin film electrode layer. 5 different protocols were given for 11 sensors, however only 5 were used for this experiment. All sensors were taken to the cleanroom, and were placed on the sputtering plate. Using the Denton Discovery 18, the sensors were placed in the sputtering machine and the pressure was dropped to 4.9 x 10^-6 Pa. Argon gas is then released into the chamber and the pressure goes up to about 1 mPa. With a rotation speed of about 18 rpm, the sputtering target of Chromium is turned on to generate a plasma while with a shutter in between the target and the sensor. The shutter is then

removed, and for 4 of the sensors, the chromium is deposited for 2 minutes, creating a film thickness of 12 A. Each of these 4 sensors were placed in the Denton Discovery 18 at different points at different times, one sensor with 2 minutes of platinum, two sensors with 6 minutes platinum, and one sensor with 12 minutes platinum. One of the two sensors with 6 minutes platinum was a 3D print, while the other sensor was acrylic. The sensors with 2 minutes and 12 minutes of platinum were also acrylic. The final protocol was for an acrylic piece, and this piece had 2 minutes titanium and 2 minutes platinum. All were vented and removed from the sputtering machine, and were taken for the preparation step.

Table 1: Sputtering times

Sensor #	Chromium (minutes)	Titanium (minutes)	Platinum (minutes)
Sensor #1	2		2
Sensor #2	2		6
Sensor #3	2		12
Sensor #4 (3D print)	2		2
Sensor #5		2	2

In this preparation step, the isolation of the electrodes and setup for the testing is required. Since the sputtering process coats the entire three electrodes evenly together, the electrodes are first isolated using the sharp tip of a pin or razor blade through the channels designed on the electrode surface. Electrical connections are verified after all three electrodes are isolated to ensure that no needles on the electrode have unintentionally been separated through a small cut. Two-part silver paste is then mixed and added to the connection between the electrode holes and the connectors shown in Figure 3 below. This fills any space between the hole and the

connector while acting as a glue to hold the pieces together. Any remaining part of the hole not filled by the connector is then filled with silver paste. 3D printed covers are then added to the surface to allow for ease of testing when adding any liquid solution on the surface. This cover acts as a well for the entire electrode, with small walls around the perimeter to maintain any solution on the surface of the electrode. Due to the supports on the stereolithography prints, these covers were sanded down to reduce the height of the well and remove any uneven wall heights due to connecting supports and poor connection points. 50 mL of UV resin was added to the surface of the electrodes on the sensor right before the cover was added to the surface. This complete setup of the sensor, connector, and cover was placed in a UV oven for 2 minutes. After 2 minutes, the sensor setup was ready for testing.

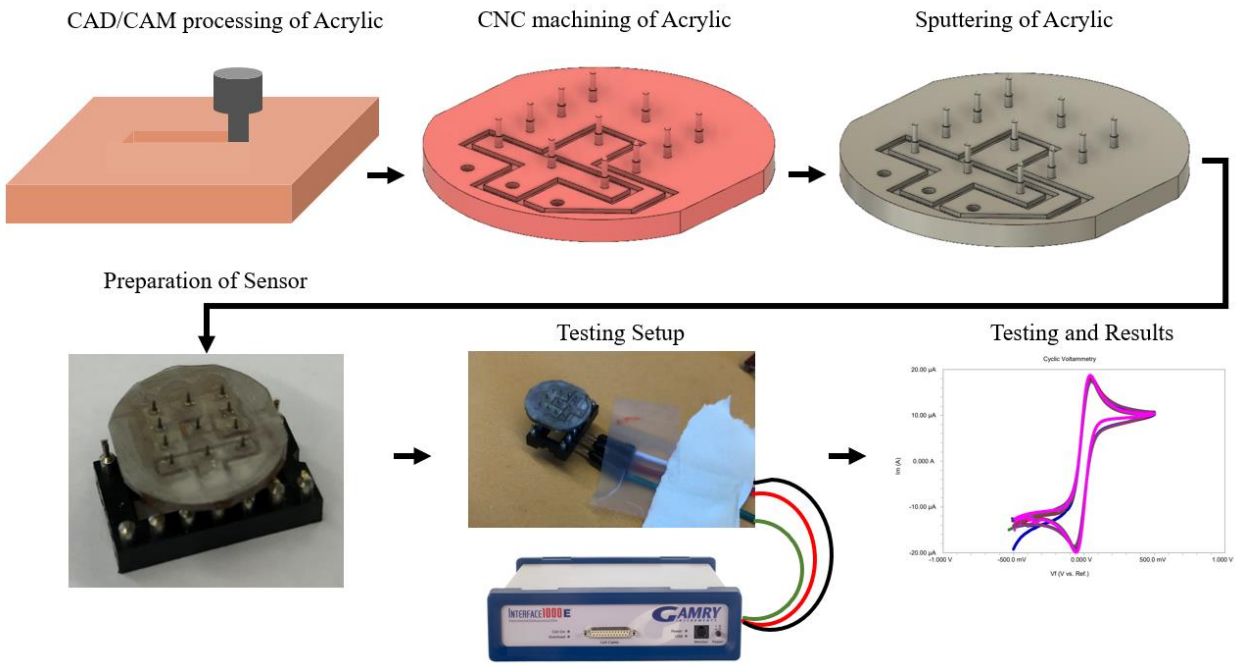

Figure 3: Process of Microneedle CNC Fabrication and Testing

The sensor was connected to the Gamry system via wire cables and alligator clips corresponding to each of the three electrodes. The wires connected to the connector is shown in Figure 3 above. The cyclic voltammetry was first tested by using a pipette to distribute 200 uL of Fe2+/Fe3+ (ferrocyanide) solution over the 11 microneedles. The surface tension helps to prevent movement of the ferrocyanide droplet, in addition to the walls of the cover. The cyclic voltammetry test is then ready to be tested. The same procedure was used for the Electrode impedance spectroscopy. The ferrocyanide was then removed from the sensor, and the surface of the sensor was cleaned with PBS. For the amperometry, a solution of 200 mM H2O2 concentration was made with 998 uL of PBS mixed with 2 uL of 90% H2O2. 198 uL of PBS was initially placed on the surface of the sensor, and for each consecutive round of measurements, 2 uL of the solution was added to the PBS until it reached a concentration of 600 uL H2O2.

CHAPTER 2. RESULTS AND DISCUSSION

The results were shown for the amperometry testing in Figures 4-7 below. For the thickness of the Platinum layer, the results seem to have a very similar slope. The biggest distinguishing feature in each of these is the maximum current that it reaches. For each sensor, the current seems to increase with increasing platinum layer thickness and decreasing hydrogen peroxide concentration. As each increment of hydrogen peroxide was added to the concentration of the PBS, the current seemed to significantly decrease from 12 to 6 minutes, and less significantly from 6 to 2 minutes of platinum. The noticeable difference between Figure 4 for 12 minutes platinum compared to the other results is that the highest concentration of hydrogen peroxide in the solution has a larger decrease in slope compared to the other concentrations. For 12 minutes of platinum, 600 mM hydrogen peroxide seemed to raise the current towards the beginning, but reached the same current as 400 mM hydrogen peroxide after about 25 seconds. Additionally, for Figure 7 with 12 minutes platinum, the PBS current is much closer to zero compared to the other two layer thicknesses. This difference is about 4.5 uA.

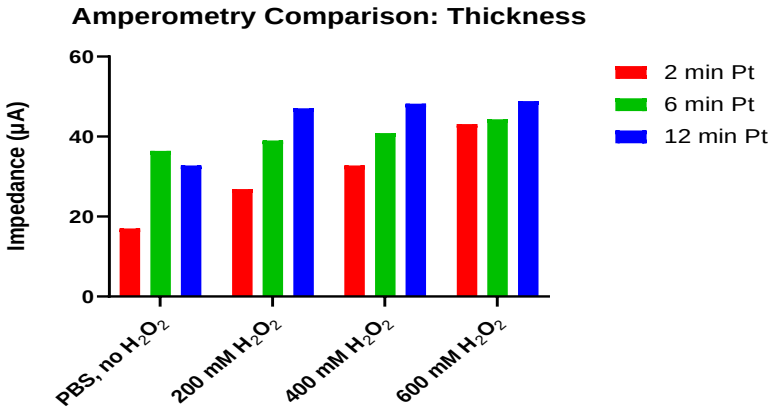

Figure 4. Amperometry Comparison: Thickness

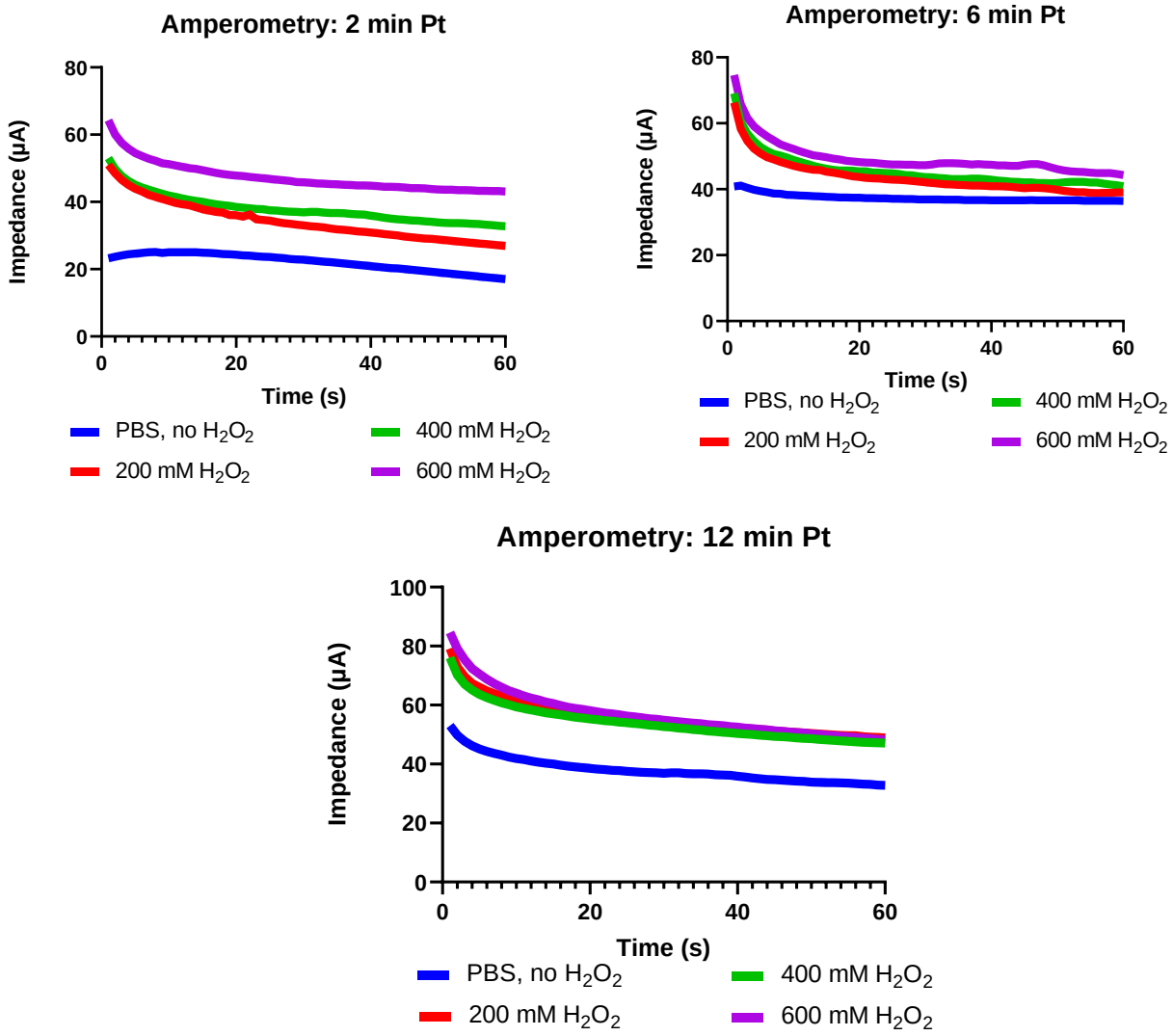

Figures 5-7. Amperometry of Electrode Layer thickness at 2, 6 and 12 minutes, correspondingly.

Considering the information for Figure 5 with Figure 8 below for the adhesion material differences, the differences can be drastic between the 400 and 600 mM H2O2 concentrations on both figures. While Figure 5 for platinum seems to follow a generally linear relationship between

concentration and current, the titanium layer does not follow that linear trend. Titanium seems to favor 400 mM concentration over 600, as the 600 mM has the largest initial concentration, but then drops below the current for the 400 mM concentration after only 4 seconds. For titanium, the 400 mM H2O2 concentration does not generate a smooth, exponentially decreasing current with time, but rather fluctuates between a zero and negative slope throughout the duration of the experiment. Additionally, the maximum current of the titanium quadrupled compared to the chromium, reaching nearly 40 uA while all platinum currents never reach above 10 uA.

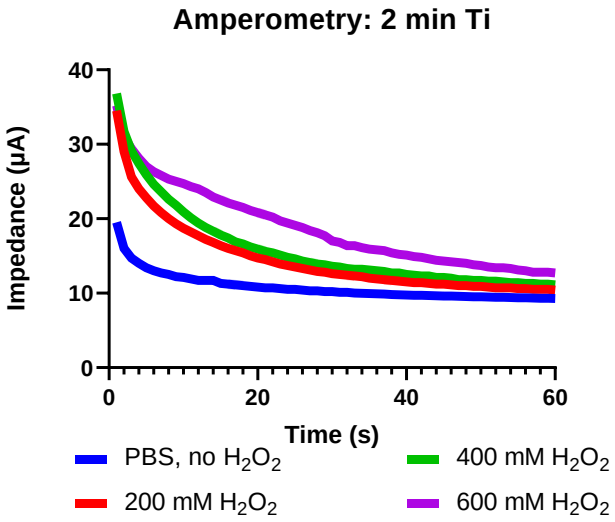

Figure 8. Amperometry, 2 min Ti

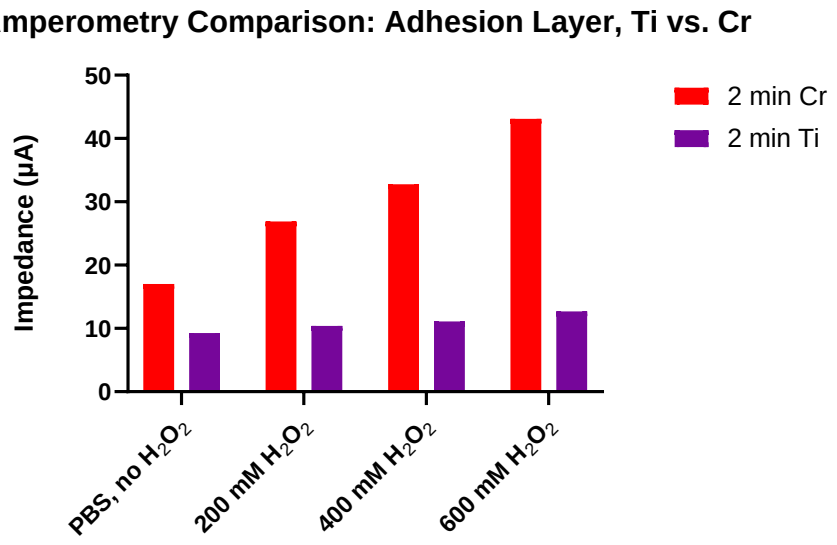

Figure 9. Amperometry Comparison: Adhesion Layer, Ti vs. Cr

In comparison to Figure 10 for the 3D printed substrate, the data follows a similar trend to the acrylic substrate. However, for the 3D printed substrate, both the 200- and 400-mM concentration reach a very similar maximum. While for the first 11 seconds, it seems as if the current will remain higher for the 200 mM concentration than the 400 mM concentration, the slope then begins to decrease and reached current measurements below the 400 mM concentration for the rest of the duration of the experiment, following a similar trend for the other platinum measurements on the CNC acrylic substrate. The difference in maximum currents is negligible. The resting current by the end of the time duration seems to be slightly larger than the platinum current, by about 1 uA.

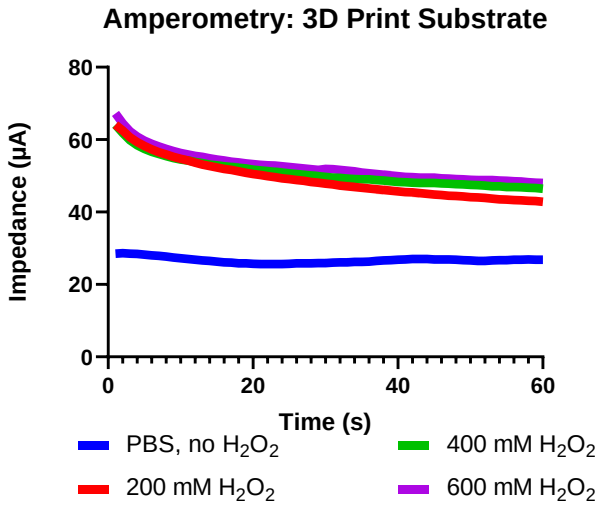

Figure 10. Amperometry, 3D Printed Substrate

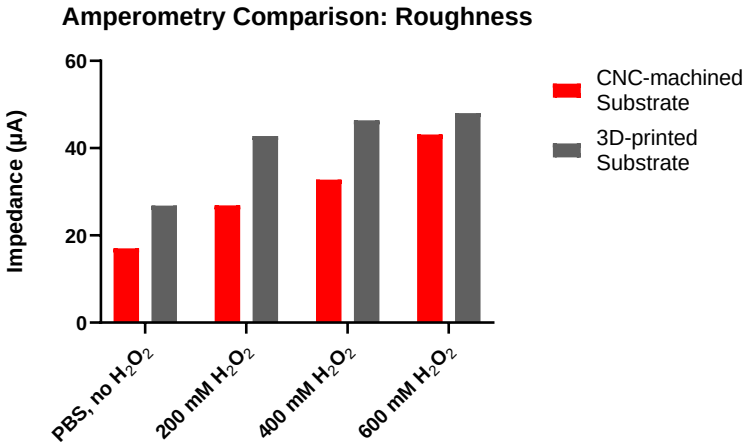

Figure 11. Amperometry Comparison: Roughness

The Potentiostatic Electrode Impedance Spectroscopy results in Figures 12-17 below were conducive of the hypothesis described in the earlier section. For the comparison of the bode and Nyquist plots of the layer thicknesses, there is an overall larger impedance for the smallest

layer thickness at every frequency measured, aligning well with the hypothesis in the previous section for the amperometry data that the thickness generates more impedance. At higher frequencies, the 6-minute layer thickness of platinum measured a higher impedance while the 12-minute layer thickness measured higher impedances at lower frequencies. Interestingly, the 2 and 12-minute thickness showed similar exponential growths on the Nyquist plot at low real impedances, but the 2 minute thickness grew at a faster rate than the 12 minute thickness at higher real impedances. If these data points were to continue, the 6 minute layer thickness showed the smallest semi-circle out of all the results, suggesting that there is less charge transfer resistance and double layer capacitance at the surface. The most important aspect of this graph is to show that the resulting current at high frequencies over 10 kHz is around 100 ohms, with 2 mins of platinum having the lowest current and 12 minutes of platinum having the highest current. However, with Figure 15, this smaller semicircle forming for Sensor #3 compared to the Sensor #2 may suggest a higher charge transfer resistance in Sensor #2. This may have been due to small impurities or imperfections in Sensor #2 as it was being handled before the beginning of the measurements. The hypothetical measurement for Sensor #2 is to remain in current responses between Sensors #1 and #3. However, this fluctuation in current response could have been due to Sensor #2 exposing the chromium layer, background noise in its connectivity to the Gamry instrument, and the shifting of the ferrocyanide on the sensor. Moving the sensor with any sudden movements can shake the ferrocyanide, unintentionally moving ions to the other electrodes, ultimately creating an unbalanced charge transfer.

In the material adhesion comparison, titanium seemed to have the least distinguishable Bode curve. With the titanium curve on the bode plot, both the phase shift and the impedance modulus seemed to have an undefined resonance range, while the low frequencies seem to be the

best range of resonance for platinum. The material adhesion shows a drastic effect on the phase shift for both, where the largest difference is at around 200 Hz when the phase shift difference is nearly 45 degrees. The titanium curve on the Nyquist plot was delayed before making the working electrode curve. While the platinum begins its working electrode curve without any resistance due to capacitance, the slow rise at the beginning of the Ti plot shows a significant amount of charge transfer resistance. Interestingly, while this amount of resistance should be evident in a decrease in current, the Bode plot for titanium shows an increase in current at higher frequencies. This titanium could be reacting directly with the ferrocyanide to create this discrepancy, creating such a large peak current in the cyclic voltammetry curve. Many theories for such a large impedance could arise from changes to the molecular structure as titanium may have reacted to the Platinum surface above it, causing a resistance in charge transfer with the ferrocyanide. Since the titanium sensor was fabricated at a different time than the other sensors, its possible that these layers may have not been sputtered properly due to the vacuum environment or length of sputter time, exposing the titanium to atmospheric air prematurely. This may have caused the titanium to be openly exposed to the surface that the ferrocyanide was in contact with, causing unintended side reactions.

For the roughness comparison between the CNC machined acrylic and the 3D printed substrate, both have similar reactions to changes in frequency. The majority of the higher frequencies show negligible differences in the resulting impedance and phase shift. For the lower frequencies, the Bode plot curve shows a higher slope with the CNC machined acrylic, showing that there are higher impedances at lower frequencies. The 3D printed curve on the Nyquist plot also shows a smaller exponential curve compared to the CNC machined substrate. A greater surface area on either one of these electrodes would allow for more binding sites, increasing the

transfer rate for the larger working electrode when an enzyme is added. Considering the potential for the rougher, CNC-machined surface to have a greater surface area, the difference in the surface area of the rougher, CNC-machined surface and the smoother, 3D-printed surface is considered negligible. The Bode plot discrepancy at the lower frequencies may have resulted in a slightly less surface resistance on the 3D print compared to the CNC-machined surface. The Werburg's constant could be slightly lower for the 3D printed surface, causing a faster decrease in slope on the Nyquist plot. Overall, there is very minimal changes to the impedance between the two surfaces, but there is less overall resistance on the 3D printed surface at lower frequencies.

Due to the nature of this experiment, this component of the experimentation was not fully developed or calculated for its Werburg's constants, as well as the Randle's circuit parameters. If this was continued, there would be much more emphasis on the analysis of the bode plot found in EIS, with proper reproducible controls to avoid noise and maintain consistency throughout the sensor samples. Equations for theoretical analysis of EID would be defined to compare with the experimental values and to help calculate the charge transfer resistance, double layer capacitance, and other ionic resistance.

Figures 12-17. Bode and Nyquist Plots of Electrode Layer Thickness, Adhesion Layer Material, and Substrate Roughness, correspondingly.

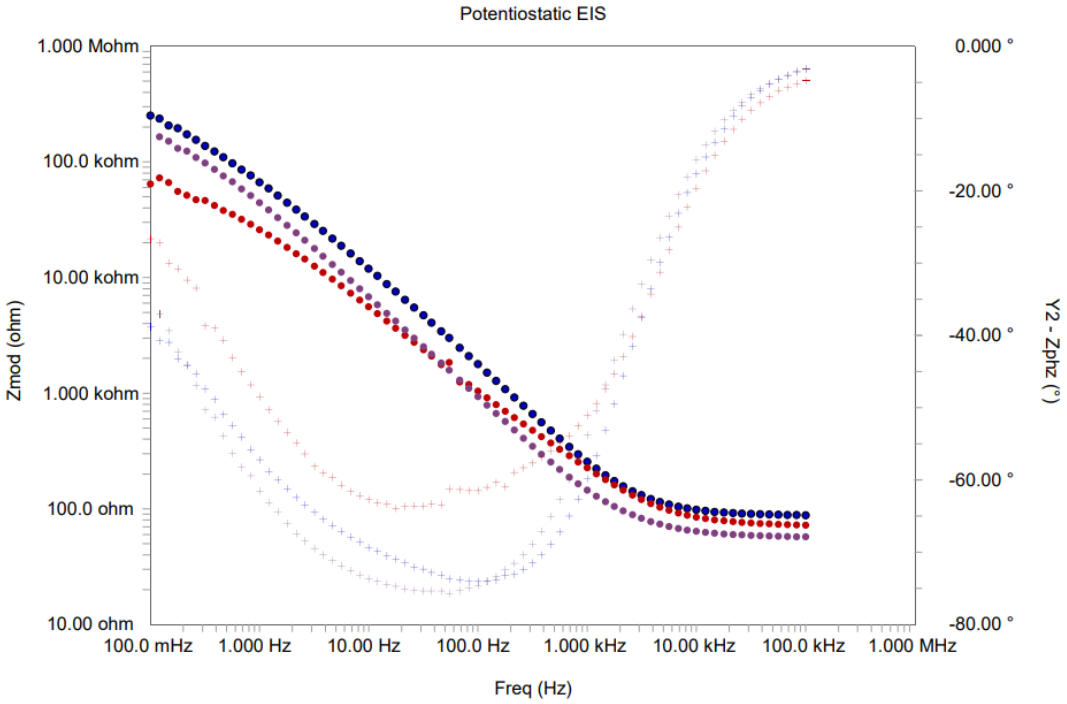
Potentiostatic EIS
1.000 Mohm
100.0 kohm
10.00 kohm
1.000 kohm
100.0 ohm
10.00 ohm
Zmod (ohm)
0.000 °
-20.00 °
-40.00 °
-60.00 °
-80.00 °
Y2 - Zphz (°)
100.0 mHz
1.000 Hz
10.00 Hz
100.0 Hz
1.000 kHz
10.00 kHz
100.0 kHz
1.000 MHz
Freq (Hz)

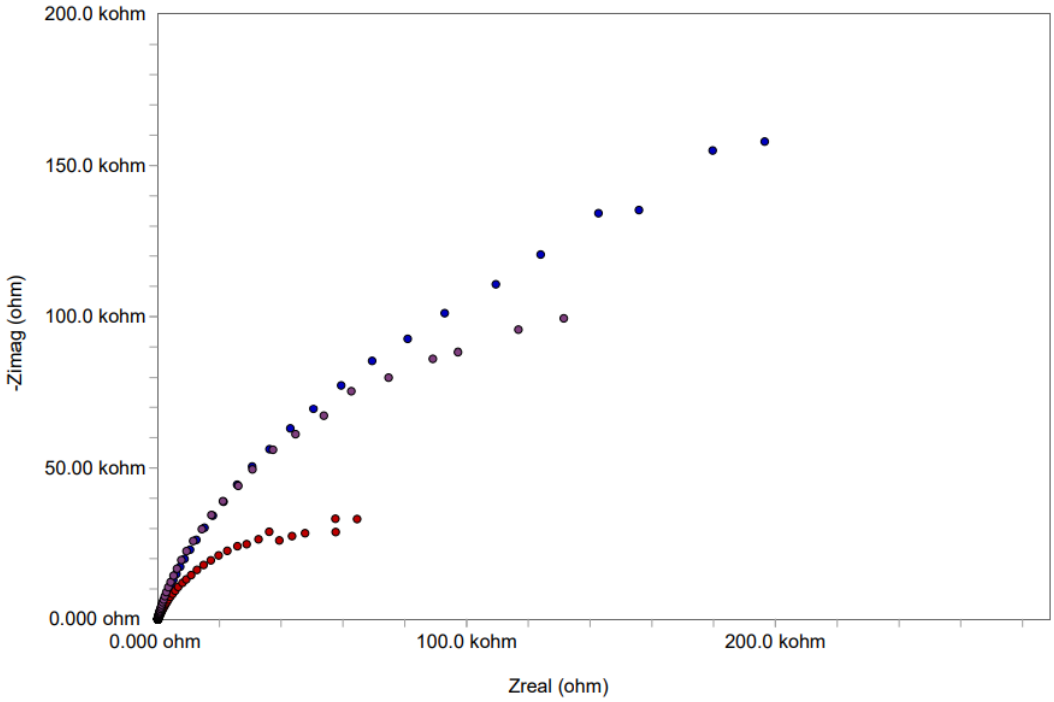
200.0 kohm
150.0 kohm
100.0 kohm
50.00 kohm
0.000 ohm
-Zimag (ohm)
0.000 ohm
100.0 kohm
200.0 kohm
Zreal (ohm)

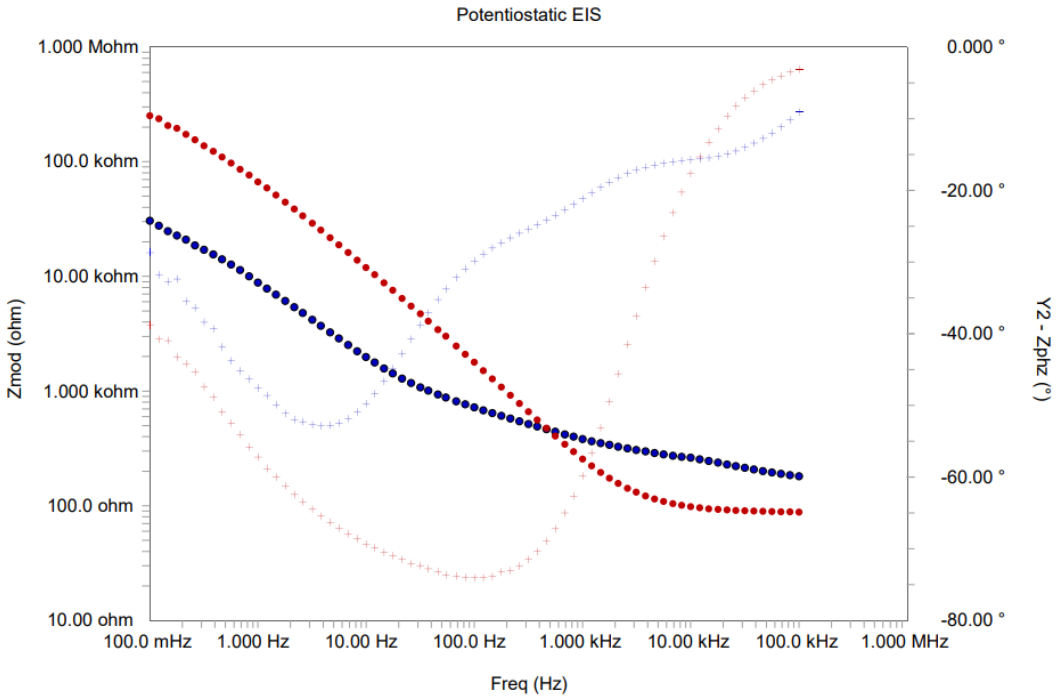
Potentiostatic EIS
1.000 Mohm
100.0 kohm
10.00 kohm
1.000 kohm
100.0 ohm
10.00 ohm
Zmod (ohm)
0.000 °
-20.00 °
-40.00 °
-60.00 °
-80.00 °
Yz - Zphz (°)
100.0 mHz
1.000 Hz
10.00 Hz
100.0 Hz
1.000 kHz
10.00 kHz
100.0 kHz
1.000 MHz
Freq (Hz)

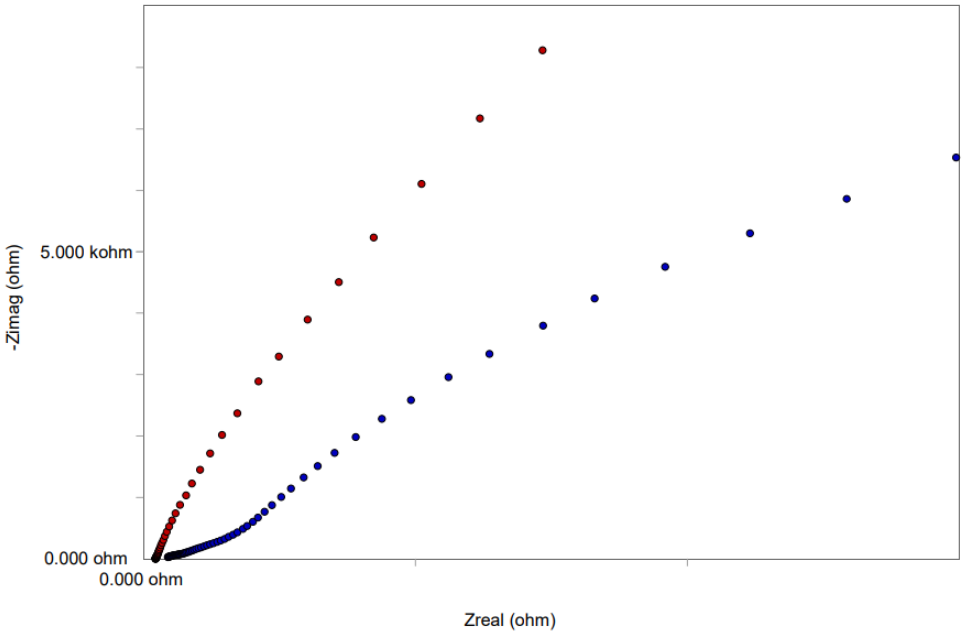
5.000 kohm
0.000 ohm
-Zimag (ohm)
0.000 ohm
Zreal (ohm)

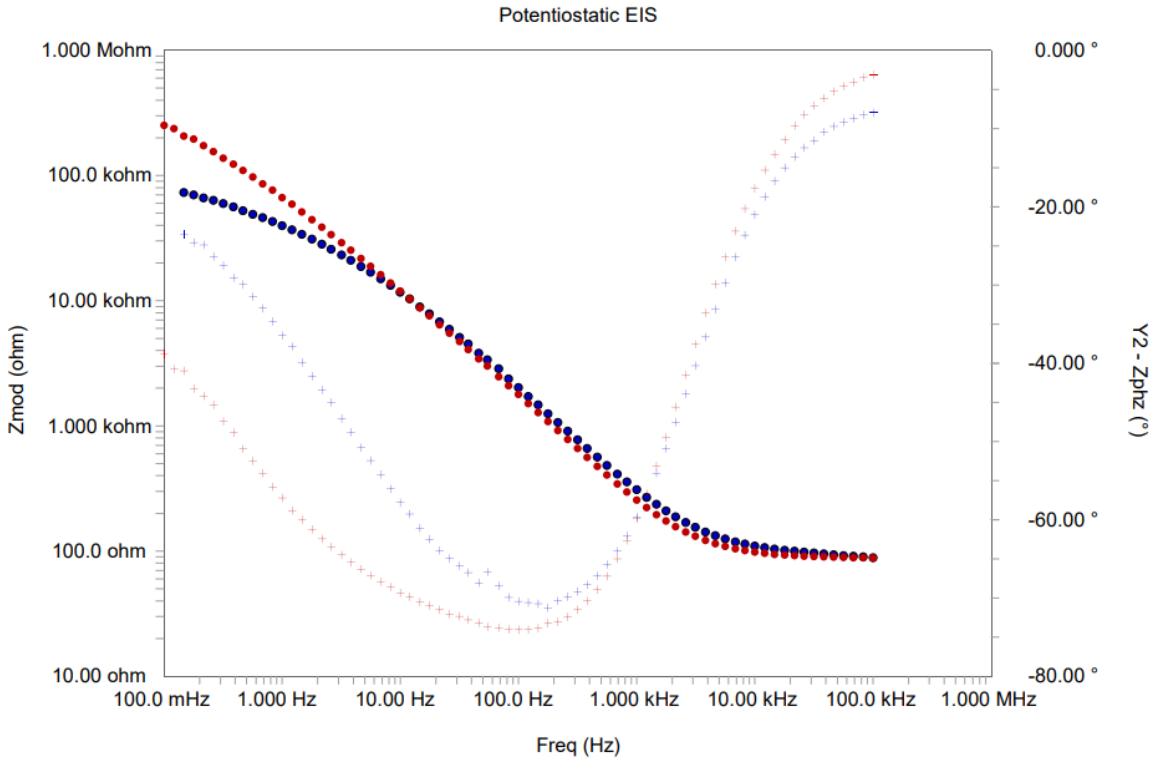
Potentiostatic EIS
1.000 Mohm
100.0 kohm
10.00 kohm
1.000 kohm
100.0 ohm
10.00 ohm
Zmod (ohm)
0.000 °
-20.00 °
-40.00 °
-60.00 °
-80.00 °
Y2 - Zphz (°)
100.0 mHz
1.000 Hz
10.00 Hz
100.0 Hz
1.000 kHz
10.00 kHz
100.0 kHz
1.000 MHz
Freq (Hz)

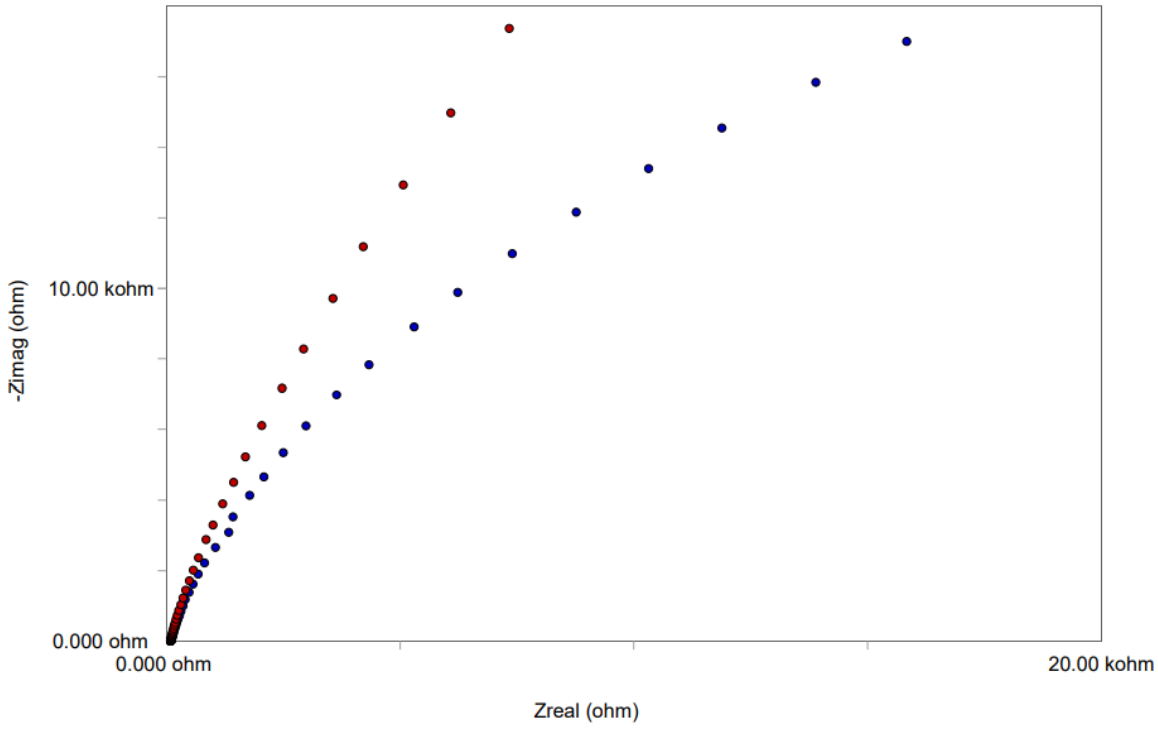
10.00 kohm
0.000 ohm
-Zimag (ohm)
0.000 ohm
20.00 kohm
Zreal (ohm)

The cyclic voltammetry curves are shown in Figures 18-20 below. For the thickness, it is shown in the different sides of the scan that there is some background noise giving some instability in the lines. In most circumstances, it is not advantageous to have background current exist within the final data and will usually be removed through interpolating the data post-experiment. However, if the potentiostat doesn't have a high sensitivity, having more background current can allow for better accuracy. These thicknesses show that the thicker the layer, the more current is going through the system. With thicker platinum layers overlaid with background noise, the Sensor #3 could have the best accuracy. However, due to the instability of the responses, this data is not reproducible and therefore should not be considered a sufficient assumption for how the thickness of platinum responds in cyclic voltammetry. Similarly, based on the EIS results, it is not surprising to see the similarities between the 3D printed surface and the CNC-machined surface. This shows that the charge transfer rate is about the same between the two.

For the adhesive comparison, there is a similar potential peak window but a wide variation in the maximum current. The peak-to-peak length is bigger in titanium. This aligns with the amperometry and EIS data for the adhesion layers, deducing the possibility that titanium causes a significantly greater impedance than chromium. This may mean that chromium may be a better adhesive layer than titanium, and should allow for more stability in the sensor. However, this may be due to changes in molecular structure, such as more bonding with platinum that can cause interfering species as a response of titanium interacting with the analyte of interest.

Figures 18-20. Cyclic Voltammetry Results for Adhesion Layer: Ti vs. Pt (top), Roughness: 3D print vs. CNC-machined substrate (middle), and Pt Thickness (bottom)

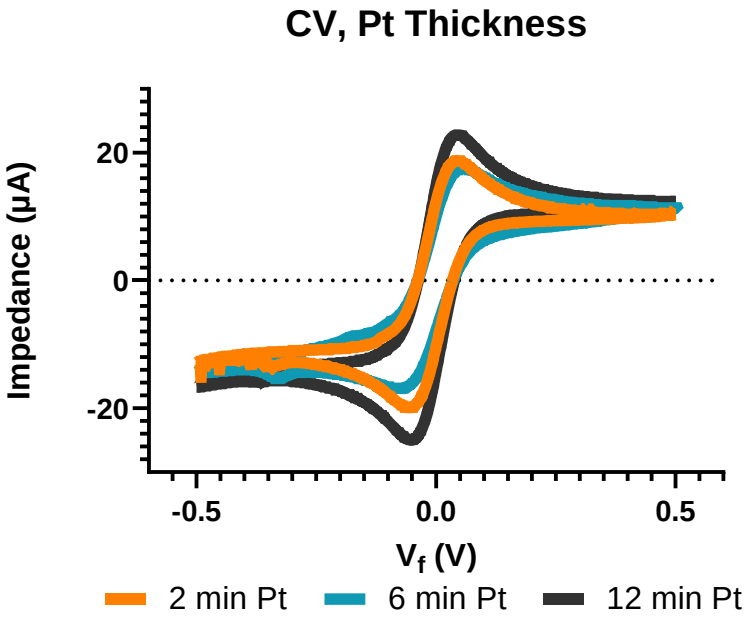
CV, Pt Thickness
Impedance (µA)
20
0
-20
-0.5
0.0
0.5
V_f (V)
2 min Pt
6 min Pt
12 min Pt

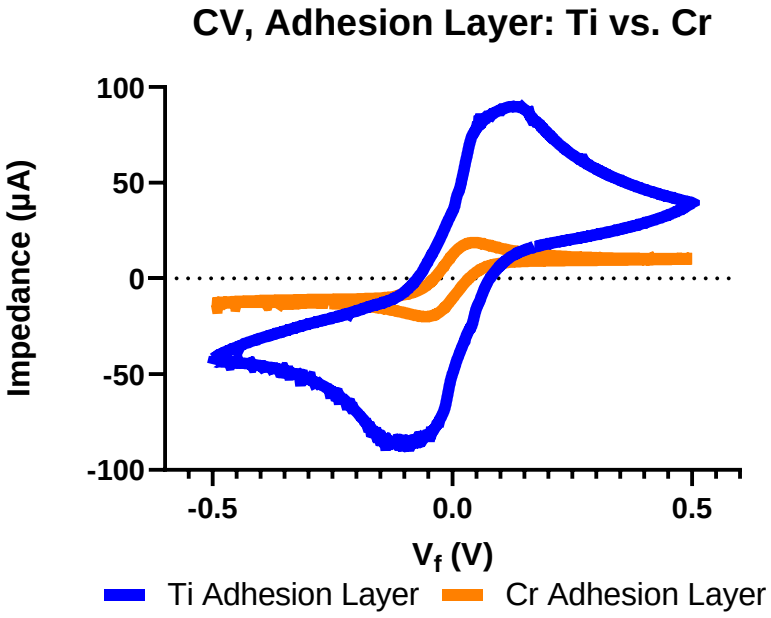
CV, Adhesion Layer: Ti vs. Cr
Impedance (µA)
100
50
0
-50
-100
-0.5
0.0
0.5
V_f (V)
Ti Adhesion Layer
Cr Adhesion Layer

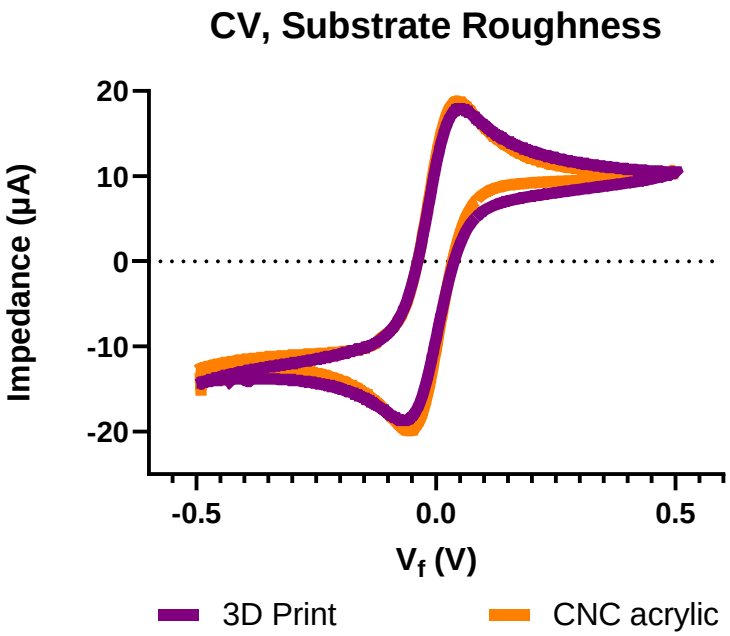
CV, Substrate Roughness
20
10
0
-10
-20
Impedance (µA)
-0.5
0.0
0.5
V_f (V)
3D Print
CNC acrylic

CHAPTER 3. CONCLUSION

In conclusion, there is a possibility for multiple discrepancies in the fabrication process that could cause unintended results, but titanium seems to be a less efficient choice for ion transfer between the target and the electrode compared to chromium. Additionally, a thicker electrode layer of platinum can cause a higher impedance on the electrode. However, the PLA and PMMA substrate did not cause discrepancies in the electrochemical functionality of the electrode. Titanium caused a substantially higher current on the electrode than chromium, suggesting that the molecular structure may have caused a competing reaction to the ion transfer with the analyte of interest. An unintended reaction to the electrode surface may have also exposed the titanium, causing the titanium to react highly with the analyte of interest. However, this is an ongoing study and more reproducibility needs to occur to confirm that these theories are how these parameters affect the interfacial charge transfer.

To further develop the feasibility of this study, a well-defined protocol needs to be set in place and tested multiple times before developing the sensor samples. This will ensure little to no user error in the fabrication of the 3D-printed or CNC-machined sensors. With adequate funding, this protocol may be established at a manufacturing facility set in a production line. Creating these reproducible microneedle sensors with the same measurable surface area for normalization will reduce any potential discrepancies between the sensors due to deviations from the fabrication protocol. If deviations were to occur from the protocol, this can be documented in component validation reports and allow for more precise traceability when obtaining final CV, EIS, or amperometry results. If any of these results were not as expected, these deviations from the protocol can be traced to make any necessary connections with the results. Unfortunately,

due to lack of time and little development on the manufacturability of the sensors, this will likely not happen until the sensors are tested and matured to a high level of confidence for production.

The goal for this study was to further understand the adhesion layer of these microneedle sensors, and these results will be a sufficient launching point for further investigation to optimizing the integrity of the electrode layer. The use of titanium and chromium will now be carefully considered in the development of these electrochemical microneedle sensors, as well as refining the interfacial charge transfer with adjusting the thickness of the electrode layer and changing the substrate material as necessary. It will also be essential to understand all the effects of the studied parameters on the mechanical features and the long-term stability of the electrodes. As these results are further refined with statistical analysis, including replicates for each parameter to have a better data analysis and more robust conclusions, the lifespan of these on-body sensors can be lengthened to enhance the quality of life of the user.

Works Cited

[1]Nascimento, C. D., Souza, E. G., Aguzzoli, C., & Cruz, R. L. (2019). Effects of oxygen on the resistivity in Au thin films with Ti-Al adhesion layer. Journal of Vacuum Science & Technology B, 37(5), 052202.

[2]Al-Nemrawi, N. K., Marques, J., Tavares, C. J., Oweis, R. J., & Al-Fandi, M. G. (2018). Synthesis and Characterization of Photocatalytic Polyurethane and Poly(Methyl Methacrylate) Microcapsules for the Controlled Release of Methotrexate. Drug Development and Industrial Pharmacy, 1–21.

[3]Forte, M.A.; Silva, R.M.; Tavares, C.J.; Silva, R.F.e. Is Poly(methyl methacrylate) (PMMA) a Suitable Substrate for ALD?: A Review. Polymers 2021, 13, 1346.

[4]H. Teymourian, F. Tehrani, K. Mahato, and J. Wang, "Lab under the skin: Microneedle based wearable devices", *Advanced Healthcare Materials*, (2021) 2002255.

[5]M.M. Sharif, M.A.M. Johari, A. Al Noman, M.I.M. Abdul Khudus, S.W. Harun, PMMA microfiber and Microball Resonator for fomaldehyde liquid sensing, Sensors and Actuators A: Physical, Volume 304, 2020, 111828, ISSN 0924-4247.

[6]Mu-Rong Yang, Ko-Shao Chen, Shao-Ta Hsu, Tzong-Zeng Wu, Fabrication and characteristics of SiOx films by plasma chemical vapor deposition of tetramethylorthosilicate, Surface and Coatings Technology, Volume 123, Issues 2–3, 2000, Pages 204-209, ISSN 0257-8972.

[7]Nguyen, Tien & Breitkopf, Cornelia. (2018). Determination of Diffusion Coefficients Using Impedance Spectroscopy Data. Journal of The Electrochemical Society. 165. E826-E831.